ELSEVIER

Nonlinear plasmonic antennas

Shakeeb Bin Hasan[1], Falk Lederer[1] and Carsten Rockstuhl[2,3,*]

[1] Institute for Condensed Matter Theory and Solid State Optics, Abbe Center of Photonics, Friedrich-Schiller-Universität Jena, Max-Wien-Platz 1, 07743 Jena, Germany
[2] Institute of Theoretical Solid State Physics, Karlsruhe Institute of Technology, 76131 Karlsruhe, Germany
[3] Institute of Nanotechnology, Karlsruhe Institute of Technology, 76021 Karlsruhe, Germany

Contrary to traditional optical elements, plasmonic antennas made from nanostructured metals permit the localization of electromagnetic fields on length scales much smaller than the wavelength of light. This results in huge amplitudes for the electromagnetic field close to the antenna being conducive for the observation of nonlinear effects already at moderate pump powers. Thus, these antennas exhibit a promising potential to achieve optical frequency conversion and all-optical control of light at the nano-scale. This opens unprecedented opportunities for ultrafast nonlinear spectroscopy, sensing devices, on-chip optical frequency conversion, nonlinear optical metamaterials, and novel photon sources. Here, we review some of the recent advances in exploiting the potential of plasmonic antennas to realize robust nonlinear applications.

Introduction

Surface plasmon polaritons (SPPs) refer to the oscillation of charge density waves resonantly coupled to the electromagnetic field at a metal–dielectric interface [1]. SPPs stand out in comparison with light in conventional all-dielectric optical elements for their confinement is not restricted by the conventional diffraction limit [2]. Therefore, SPPs can be localized and guided deeply sub-wavelength, which promises a viable route toward the realization of ultra-compact waveguides and antennas for integrated optics [1,3,4].

In addition to realizing compact optical elements, the deep sub-wavelength confinement of SPPs is accompanied by huge near-field amplitudes of the electromagnetic fields. This permits the observation of nonlinear effects at moderate power levels even though the interaction volume might be very small. Mathematically this means that the induced polarization in the medium ceases to be linearly related to the electric field. Restricting our consideration for the moment to a non-resonant interaction of light with homogenous matter, the resulting nonlinear polarization can be described by higher order Taylor terms as [5]

$$P_i(t) = \varepsilon_0 \int_0^\infty R_{ij}^{(1)}(\tau) E_j(\vec{r}, t-\tau) d\tau + \varepsilon_0 [\chi_{ijk}^{(2)} E_j(t) E_k(t) + \chi_{ijkl}^{(3)} E_j(t) E_k(t) E_l(t) + \ldots], \quad (1)$$

where the indices run over the Cartesian coordinates, ε_0 is the permittivity of free space, $R_{ij}^{(1)}(t)$ the response tensor whose Fourier transform yields the susceptibility tensor $\chi_{ij}^{(1)}(\omega)$ of a linear, dispersive medium, whereas $\chi_{ijk}^{(2)}$ and $\chi_{ijkl}^{(3)}$ are the non-dispersive second- (quadratic) and third-order (cubic) nonlinear susceptibility tensors, respectively. This substantial simplification of vanishing nonlinear dispersion can be made if all frequencies involved are far below any resonance frequency of the nonlinear medium and Kleinman symmetry holds [5]. In this case both tensors are real-valued. While the cubic nonlinearity is present in all media in varying strength, the quadratic term vanishes in bulk centrosymmetric media [5]. The nonlinear polarization (Eq. (1)) includes the most prominent effects as parametric frequency mixing, including parametric amplification, and self-phase modulation [5–9].

*Corresponding author:. Rockstuhl, C. (carsten.rockstuhl@kit.edu)

http://dx.doi.org/10.1016/j.mattod.2014.05.009

For dielectric optical media these nonlinear effects have been extensively investigated and experimentally observed in the past [5]. However, much remains to be explored in plasmonic systems, which can enhance the nonlinear response both in the surrounding dielectric media (sometimes called extrinsic response), and in the metal itself, which forms the plasmonic systems (sometimes called intrinsic response). This is evidently caused by the substantial field enhancement for moderate input pump powers. Prominent examples are quadratic nonlinear effects such as second harmonic generation (SHG) due to symmetry breaking at the surface of centrosymmetric media [10–12] as well as a quadratic response in metals which emerges from a full hydrodynamic model for the electron gas [13–16]. In particular, the latter aspect has attracted a considerable deal of research interest because metals being centrosymmetric media are not expected to generate a bulk second order nonlinear response. However, if both intrinsic and extrinsic sources of nonlinearity are present, usually the latter turns out to be stronger. Moving beyond classical limits, nonlinear effects also arise when quantum mechanical effects become prominent. This generally occurs when plasmonic antennas are placed sufficiently close enough that quantum tunneling effects become significant [17–19] or while considering the resonant interaction of plasmonic antennas with quantum systems [20,21].

Although all the aforementioned issues are scientifically interesting and subject to current research, we will restrict the scope of this review to nonlinear effects in plasmonic antennas that can be described by the phenomenological model of Eq. (1). In particular, we will be interested in the opportunities offered by plasmonic antennas to tailor and electromagnetic fields at nanoscale for significantly enhancing the nonlinear effects. To provide a broader overview, we will begin with a brief introduction to the resonant localization of light by plasmonic antennas. A snapshot of recent trends and developments pertaining to the observation nonlinear effects in various systems will follow this.

Plasmonic antenna resonances

The localization of light evoked by plasmonic elements is best introduced by the referential example of a small sphere. According to Mie theory, the field scattered by a metallic sphere of radius much smaller than the wavelength of the incident light corresponds to that of an induced electric dipole moment inside the sphere. The induced dipole moment can be resonantly excited when the so-called Fröhlich condition is satisfied which requires the permittivity of surrounding dielectric to be opposite in sign and twice as large in magnitude as the permittivity of metal [22]. This results in localization and enhancement of light at the interface between a sub-wavelength metallic sphere and the surrounding dielectric medium. Further modification to the basic spherical geometry such as spherical core–shells [23], ellipsoids, cylinders [22], discs [21] or even coupled spheres [24] have also been analytically described. More advanced shapes such as bow-tie structures [25] lead to similar resonant scattering of light with different degrees of freedom to tune the resonance frequency. However, a description of their properties usually requires rigorous numerical treatment [26–29]. To circumvent all constraints imposed by specific geometries, a recent study proposed to employ an evolutionary algorithm to devise plasmonic particles of arbitrary shapes in order to achieve resonances at frequencies on demand [30].

Apart from the particles discussed above, the so-called plasmonic wires can also achieve plasmonic localization of light. They are essentially metallic waveguides of finite length. As such, they form a Fabry–Perot (FP) cavity where the excited propagating SPP mode sustained by the metallic waveguide oscillates back and forth between the waveguide terminations [31,32]. Being a cavity, the structure resonates when the resonance condition of a FP cavity is met. This requires the round-trip phase accumulated by the guided plasmonic mode to be an integer multiple of 2π. Like plasmonic particles, plasmonic wires also come in different flavors such as cylindrical [31], center-fed [33] and also in more complicated geometries such as split-rings [34,35]. This provides various degrees of freedom to tailor their response according to specific needs.

Nonlinear frequency conversion

Departing from the ability to tailor the electromagnetic response in linear optics, the most common manifestation of nonlinear effects in plasmonic antennas is the conversion of the frequency of light to second harmonic (SH) in a quadratic medium and third harmonic (TH) when the material exhibits a cubic nonlinear response. A natural strategy for harvesting the nonlinear potential of plasmonic antennas is to tune the input pump to the antenna resonance, although non-resonant pumping can also enhance nonlinear conversion if the generated harmonic meets the antenna resonance [36]. Most commonly used antennas for nonlinear frequency conversion include spheres [37–39], core–shells [40–43], nano-wires [44–46], bow-ties [6,8,9], asymmetric L-shaped particles [47,48] and split-rings [14,49–51], composite geometries such as dimers [52–54], and clusters configurations [55,56].

From a theoretical standpoint, plasmonic antennas also present an interesting platform to study an artificially induced quadratic nonlinear response in metals. As mentioned in the introduction, the second order term in Eq. (1) vanishes in centrosymmetric bulk media. Symmetry breaking at the surface can nevertheless act as a weak SH dipole source [10–12]. In structured media such as spheres, it is also possible to induce a bulk nonlinear quadratic response due to the excitation of higher-order multipole moments such as the magnetic dipole or the electric quadrupole [39,57]. Asymmetric plasmonic elements, such as L-shaped [58] and split-ring [35,59] antennas, can also be engineered to exhibit an induced non-centrosymmetric response [47,48,50,51,60,61]. In case of split-ring resonators, for instance, the source of bulk quadratic effects has been long suspected to be the magnetic and associated electric quadrupolar moments [49–51,61,62].

We consider spherical plasmonic core–shell (CS) particles as an example of a practical scheme for realizing antennas that serve as a source for high harmonic generation. Their localized resonance can be easily tuned by modifying the ratio between inner and outer radii of the core and shell, respectively [23]. This allows greater flexibility compared to spherical particles whose resonance in the sub-wavelength regime can only be engineered by the physical properties of the surrounding medium [22]. The nonlinear frequency conversion from CS particles has been investigated both theoretically and experimentally [40–42]. Figure 1a shows the CS geometry made up of a gold shell and a $BaTiO_3$ core that exhibits a strong quadratic nonlinear response which was used in Ref. [40] as a tunable source of SH generation (SHG). Figure 1b

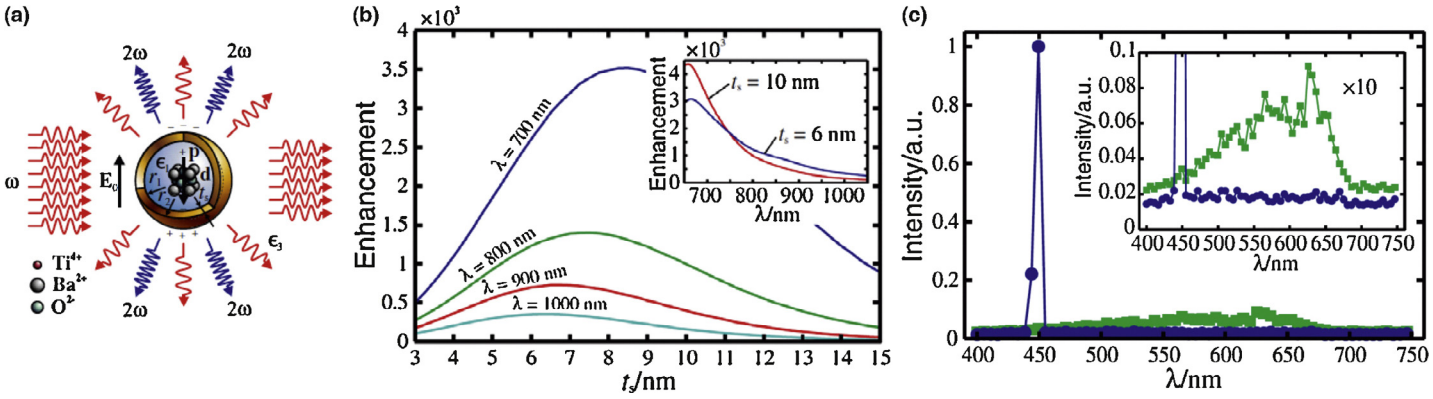

FIGURE 1

Core–shell geometry for enhanced SHG. (a) Schematic of the geometry made of a metallic shell and a $BaTiO_3$ core with a $\chi^{(2)}$ response. (b) SH emission enhancement (with respect to a planar gold film of the shell thickness embedded in $BaTiO_3$) as function of the shell thickness for different wavelengths. The inset shows the same for two different shell thicknesses as a function of the incident wavelength. (c) Normalized measured SH intensity from an Au–$BaTiO_3$ CS particle (blue) of core radius 100 nm and a gold sphere of radius 200 nm (green). Inset shows the zoomed image. Figures adapted from Ref. [40].

plots the calculated SH emission enhancement compared to a planar gold film in $BaTiO_3$ of same shell thickness for various values of excitation wavelength. Measurements were also made on fabricated CS particles of core radius 100 nm, shown in the blue curve of Fig. 1c. Also shown for comparison is the SH intensity recorded from a gold sphere of radius 200 nm in the green curve. Beyond the spherical geometry, CS nano-wires have also been realized where the length of the wire is another degree of freedom for tuning the antenna resonance [43].

Furthermore, a high frequency conversion efficiency of plasmonic structures has been observed in antennas exhibiting Fano resonance [54,56]. A Fano resonance is a resonant scattering phenomenon characterized by an asymmetric line-shape. Far-field interference between a continuum of non-resonant modes and a resonant (bright) mode gives rise to the asymmetric line-shape [63] which is characterized by enhancement or suppression of far-field scattering depending on the phase difference between the interacting modes. In the case of scattering suppression, that is destructive interference, the energy gets strongly localized in the near-field of the antenna. Recently Thyagarajan *et al.* exploited this feature by proposing silver heptamer structures. They were engineered to sustain a Fano resonance at FH and a bright scattering resonance at the corresponding SH [56]. Figure 2a shows the numerically (blue) and experimentally (red) obtained scattering spectrum of the designed heptamer structure (inset) which exhibits a Fano-resonance at λ = 800 nm and a scattering resonance at λ = 400 nm. Figure 2b shows the measured normalized SH power for different incident wavelengths and structures as a function of incident power. Other structures considered for comparison are a dipole antenna (DA) and a double resonance antenna (DRA). SH power measured for the heptamer excited at Fano-resonance (λ = 800 nm) can be seen to be superior over other cases.

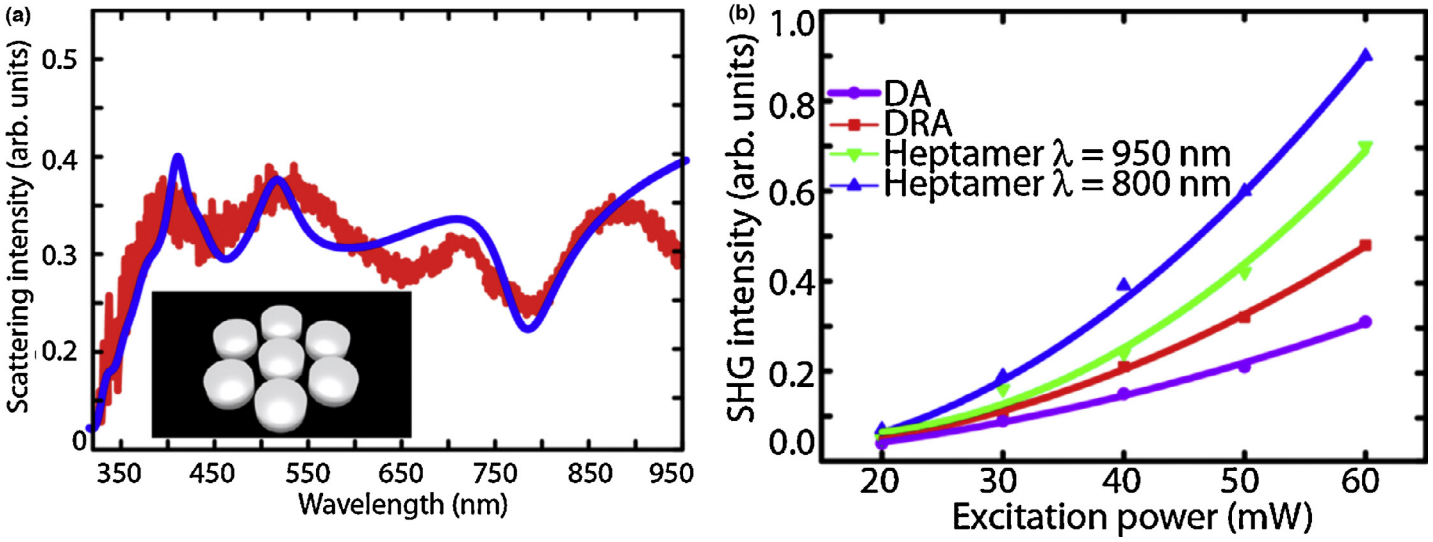

FIGURE 2

Enhanced SHG at a heptamer structure with Fano resonance. (a) Simulated (blue) and measured (red) scattered intensity spectrum. (b) Normalized measured SH intensity from a variety of structures at various excitation wavelengths as a function of excitation power. The heptamer configuration excited at the Fano resonance (λ = 800 nm) is clearly seen to be superior. Figures adapted from Ref. [56].

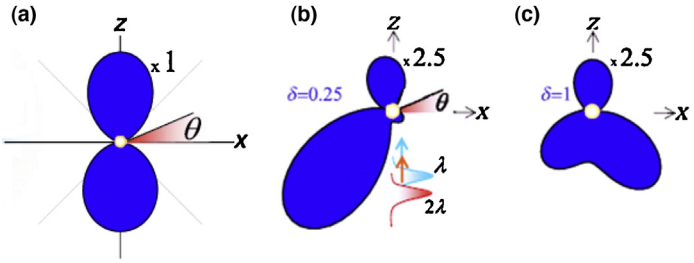

FIGURE 3

Coherent control of degenerated parametric up- and down-conversion at a gold cylinder. (a) Linearly scattered radiation profile of the signal beam at $\lambda = 532$ nm. (b) Variation of scattered radiation profile of the signal in the presence of control beam at 2λ with a phase delay $\delta = 0.25$. (c) $\delta = 1$ (c). Figures adapted from Ref. [64].

Apart from higher harmonic generation, parametric nonlinear interactions provide a rich set of tools to manipulate the nonlinear response. In the present degenerate scheme, the incident illumination is composed of both the fundamental and a higher harmonic. The outcome of nonlinear interaction at either frequency is determined by the relative phase difference between the interacting harmonics [5]. Therefore, either the FH or SH can be used as a control beam to manipulate the response of the other. This was recently exploited by Rodrigo *et al.* to study coherent control of the scattered intensity and directivity of the plasmonic antennas due to intrinsic quadratic nonlinear effects [64]. Figure 3a shows the linearly scattered radiation profile of a 2D gold cylinder when illuminated by a signal beam of amplitude E_s at wavelength $\lambda = 532$ nm. A control beam of amplitude E_c that is proportional to $E_s e^{(i\pi\delta)}$ is now introduced at 2λ with a phase delay δ with respect to the signal. Figure 3b,c show the nonlinear control in variation of scattering profile as a function of phase delay.

Multi-resonant antennas

We have seen that plasmonic antennas can serve as an efficient platform for higher harmonic generation and coherent control. To further enhance the efficiency of nonlinear frequency mixing, several innovative schemes have been recently proposed to devise structures that resonate at more than one of the frequencies involved in the nonlinear interaction [7,65–67].

We begin with the most intuitive design to implement multi-resonant antennas consisting of discrete components, each of which resonates at one of the frequencies involved [65,66]. As an example, Fig. 4a shows the schematic sketch of a geometry proposed in Ref. [65] and the electric field amplitude at the wavelength of the nonlinearly generated polarization. Two gold nanowires each with their own half-wavelength resonances are separated by a small gap (20 nm). The short arm resonates at $\lambda_1 = 780$ nm while the longer one at $\lambda_2 = 1100$ nm. The antennas are embedded in indium tin oxide (ITO) that possesses a strong cubic nonlinear response. Figure 4b plots the spectrally resolved square of the electric field enhancement at a distance of 1 nm apart from the terminations of the antennas while considering each antenna individually. In the combined structure a distance of 20 nm separates the two antennas such that the resonances tailored by adjusting the individual antennas remain largely unaffected. Consequently, a field enhancement in-between the antennas can now be observed at both wavelengths involved in the nonlinear process (Fig. 4b).

Illuminating the structure simultaneously with pumps at half-wavelength resonances of each antenna arm leads to an efficient cubic four-wave mixing (FWM) process in spatial domains where the electric fields overlap. This process induces a nonlinear polarization which radiates at the angular frequency $\omega_3 = 2\omega_1 - \omega_2$, where ω_1 and ω_2 correspond to the incident pump frequencies. Figure 4c plots the strength of nonlinear polarization as a function of spectral detuning from the half-wavelength resonances of each antenna arm. It shows that the conversion process is most efficient when the two incident wavelengths are resonant with the two antenna arms. Therefore, combining multiple antennas that sustain resonances at different frequencies and ensuring simultaneously a sufficiently good spatial overlap in the excited modes is a viable route to enhance the efficiency of nonlinear processes involving multiple frequencies.

Another way to enhance nonlinear interactions consists in designing broadband antennas whose operating bandwidth encompasses all the frequencies involved in nonlinear interactions [7,68].

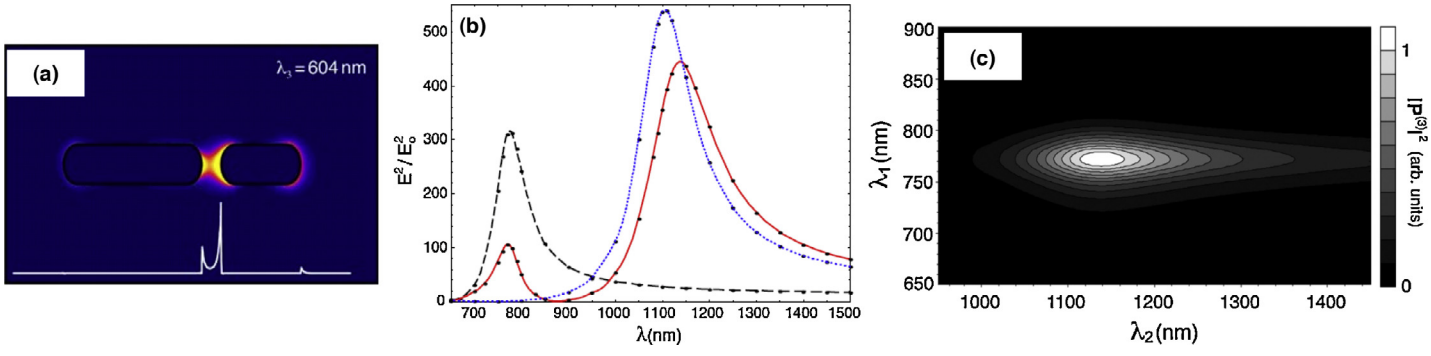

FIGURE 4

Four-wave mixing at two adjacent nanoantennas. (a) Electric field amplitude of a plasmonic antenna at wavelength λ_3 of nonlinearly generated polarization. The length of the two arms is adapted so that each sustains resonance at pump wavelengths λ_1 and λ_2, respectively. (b) Linear field enhancement at antenna terminations: short arm (black), large arm (blue), and both arms placed in close vicinity (red). Combining both arms provides a field enhancement at multiple wavelengths involved in the nonlinear process. (c) Variation of nonlinear polarization amplitude at $1/\lambda_3 = 2/\lambda_1 - 1/\lambda_2$ as a function of pump wavelengths λ_1 and λ_2. For a doubly resonant structure ($\lambda_1 = 780$ nm and $\lambda_2 = 1100$ nm) the generated polarization tends to be maximal around resonance. Figures adapted from Ref. [65].

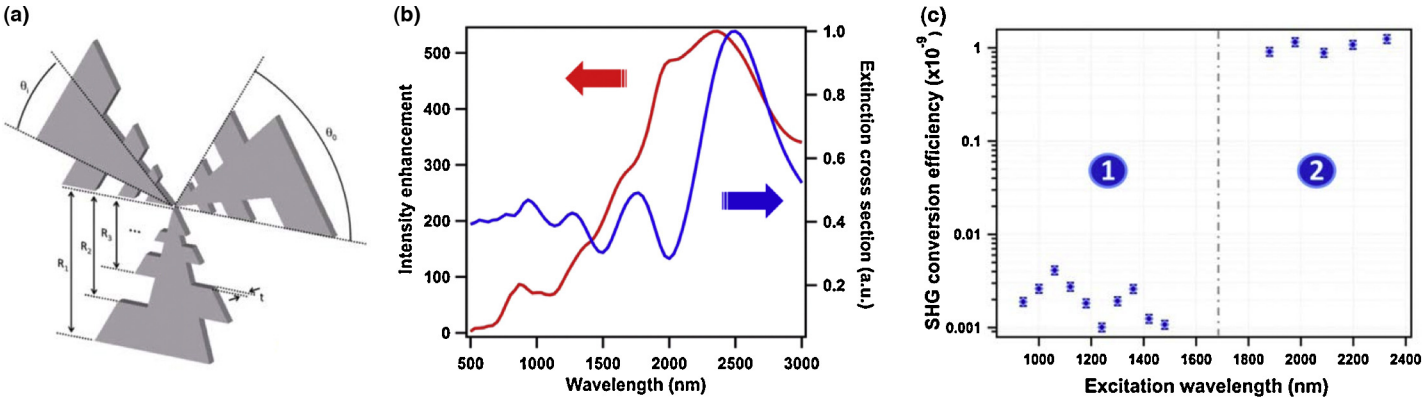

FIGURE 5

The log-periodic trapezoidal antenna for broadband SHG. (a) Schematic of the antenna. (b) Linear extinction spectrum (blue) and intensity enhancement (red) at the center point of the trapezoidal antennas as a function of the incident wavelength. The extinction spectrum never approaches zero due to closely located resonances of each arm of the trapezoidal antenna. (c) Second harmonic conversion efficiency as a function of incident wavelength. High conversion efficiency across an extended spectral range is observed due to broadband linear response. Figures adapted from Ref. [7].

As an example, Fig. 5a shows log-periodic trapezoidal antenna geometry employed to realize an efficient source of SH light [7]. The antenna is made up of arms or teeth with successively varying length, which provide half-wavelength resonances over a broad frequency spectrum. Figure 5b plots the numerically computed extinction cross-section (blue) and intensity enhancement (red) at the center of the three antenna tips shown in Fig. 5a. Four resonance peaks can be identified in the extinction spectrum shown in Fig. 5b, which are closely located in frequency to keep the extinction cross-section from approaching to zero. The intensity enhancement, however, is not uniform and is seen to decrease from around 535 near $\lambda = 2400$ nm to almost 80 for the smallest wavelength resonance around $\lambda = 933$ nm. Figure 5c shows the experimentally measured SH conversion efficiency when the antenna is illuminated by an incident pump of uniform power. As expected, we observe a huge disparity in the conversion efficiency between longer excitation wavelengths to shorter ones due to variation in intensity enhancement factor at the corresponding SH. A weak spatial overlap between the fields at FH and SH is also partly to blame for smaller conversion efficiencies at shorter wavelengths [7]. Nevertheless, the broadband resonance sustained by the antenna clearly translates into a broadband SH enhancement.

Cylindrical nano-wires are among the referential plasmonic antennas extensively investigated both experimentally and by semi-analytical means [31,32]. By proposing to exploit the shape of terminal caps as an extra degree of design freedom, it was recently shown that they offer substantial possibilities for enhancing the nonlinear response of the system [67]. Figure 6a shows a sketch of the cylindrical antenna terminated by spheroidal caps as considered in Ref. [67]. The reflection phase jump of the SPP mode guided by the cylinder at the termination sensitively depends upon the cap geometry and plays a crucial role in determining the FP resonance sustained by the antenna [69]. Therefore, the length of the antenna and the semi-axis (along the antenna axis) were both varied to obtain antenna configurations which sustain FP resonances of different orders at FH and SH frequencies.

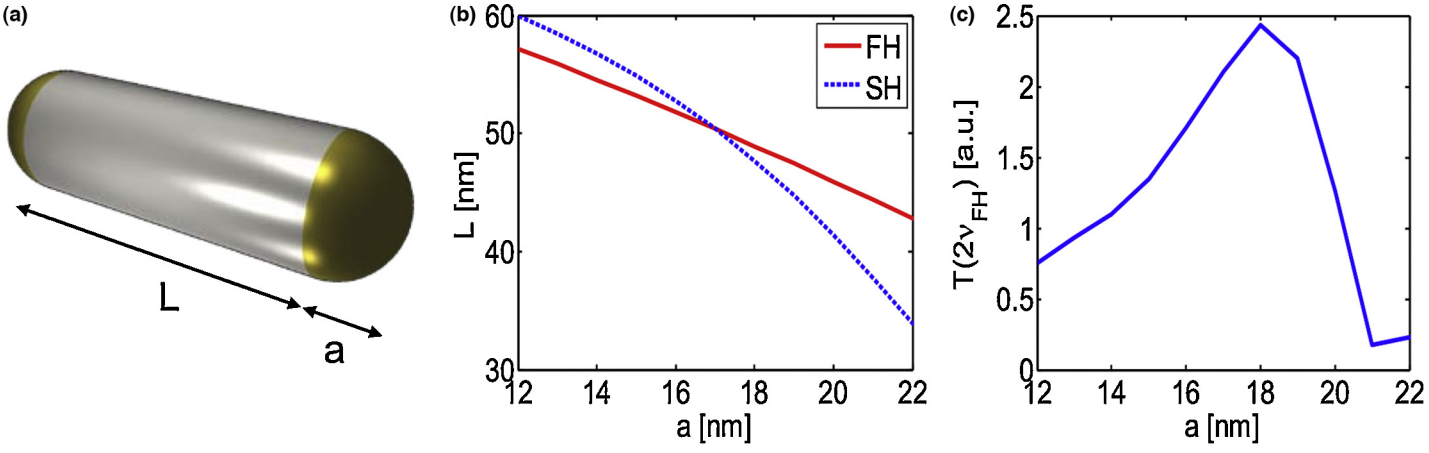

FIGURE 6

Nanowire antenna with semi-spheroidal caps for enhanced SHG. (a) Schematic of a symmetric antenna; L – wire length; a – semi-axis. (b) Antenna resonances for varying length and semi-axis for the FH (red) and the SH (blue) frequency at a fundamental frequency of $\nu_{FH} = 277$ THz. (c) Rigorously computed SH transmission spectrum through an array of antennas for a structure that is always resonant at FH according to (b) but resonant at SH for a semi-axis of $a = 17$ nm only. The nonlinear conversion is largely enhanced when the antenna is doubly resonant. Figures adapted from Ref. [67].

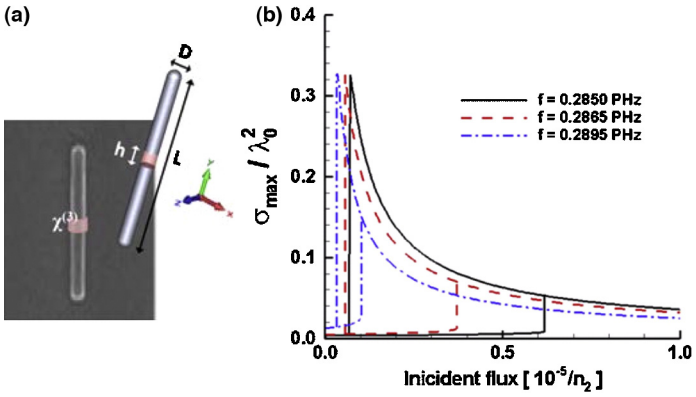

FIGURE 7

Enhanced bistability in a center-fed plasmonic antenna. (a) Schematic sketch of the antenna. (b) Normalized scattering maximum for different illumination frequencies as a function of normalized incident intensity (flux) of the plane wave. Bistable states are seen to form for each illumination frequency. Figures adapted from Ref. [71].

Figure 6b plots the geometrical configuration for which either FH (red) or SH (blue) are resonant when the antenna is excited at a pump frequency of $\nu = 277$ THz. For the specific case corresponding to $a = 17$ nm, however, the antenna sustains FP resonances at both FH and SH. Following the FH resonant configuration (red) shown in Fig. 6b, full-wave simulations based on the Finite-Difference Time-Domain method where performed to obtain the transmission at the SH from an antenna array illuminated at $\nu = 277$ THz. The results are shown in Fig. 6c. An order of magnitude enhancement can be recognized around the doubly resonant scheme when $a = 17$ nm. This result confirms the superiority of this specific antenna geometry over the configuration resonant only at pump frequency.

Intensity modulation and phase conjugation

Apart from frequency conversion processes discussed above, there are degenerate nonlinear effects, which are observed at the very incident frequency. The cubic nonlinearity, for instance, yields degenerate four-wave mixing manifesting itself in the optical Kerr effect where the input field experiences self-phase modulation, which results in an intensity dependent refractive index [5]. This can lead to optically tunable and bistable [70] plasmonic antennas being potentially useful as all-optical switches and memories [71–75].

Using the center-fed plasmonic antenna as shown in Fig. 7a, Chen *et al.* demonstrated a bistable device by exploiting nonlinearity of the dielectric feed [71]. The scattering resonance of center-fed plasmonic antennas can be systematically tuned by engineering the suitably defined impedance of the feed element [33]. Strong near-field coupling between the arms across the feed gap causes a strong field enhancement inside the gap. At resonance, the intensity inside the gap increases up to four orders of magnitude when compared to the incident flux. This leads to a bistable scattering response, which can be seen, from hysteresis in the scattering peak observed for different illumination frequencies as a function of incident power flux shown in Fig. 7b.

Apart from tuning resonances, spatial manipulation of the radiation pattern is another important task for antennas to efficiently steer the incident energy into a preferred direction. One well established design is the plasmonic Yagi-Uda geometry, which has been demonstrated to achieve directional control at optical frequencies [76,77]. However, a substantial improvement of this design is due to its applicability over a wide spectral range without physically modifying the geometry. Maksymov *et al.* have proposed such a Yagi-Uda scheme where a semiconductor load is used to feed the dipole element as shown in Fig. 8a [78]. The permittivity of the semi-conductor load is defined by the free carrier density, which in turn depends on the electric field intensity in the load. Therefore, the scattering response of the antenna can be manipulated by illuminating the feed element with a laser beam. Figure 8b shows the far-field angular power spectrum when illuminated at $\lambda = 1$ μm. The variation of power along the direction of maximum power flux is shown in Fig. 8c as a function of intensity in the semiconductor load. A closed loop pattern results

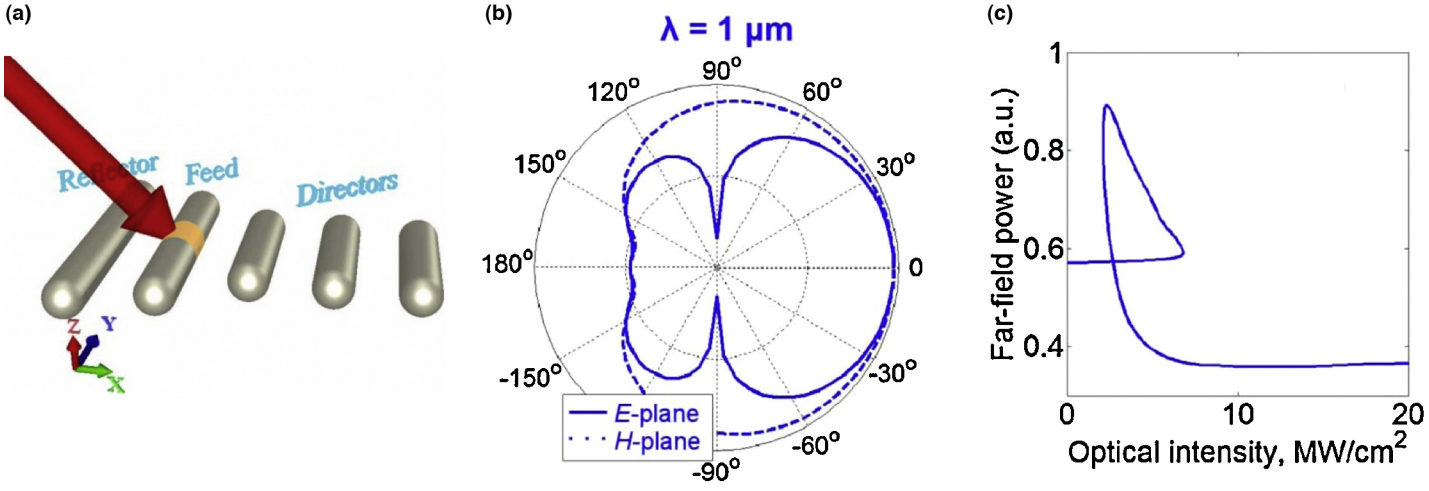

FIGURE 8

Plasmonic Yagi-Uda antenna with a dipole feed element. (a) Schematic of the antenna. (b) Far-field angular spectrum of radiated power in the E- (solid) and the H-plane (dashed) curve. (c) Maximum far-field power as a function of optical intensity in the feed. A closed loop pattern is formed showing the bistable behavior of antenna. Figures adapted from Ref. [78].

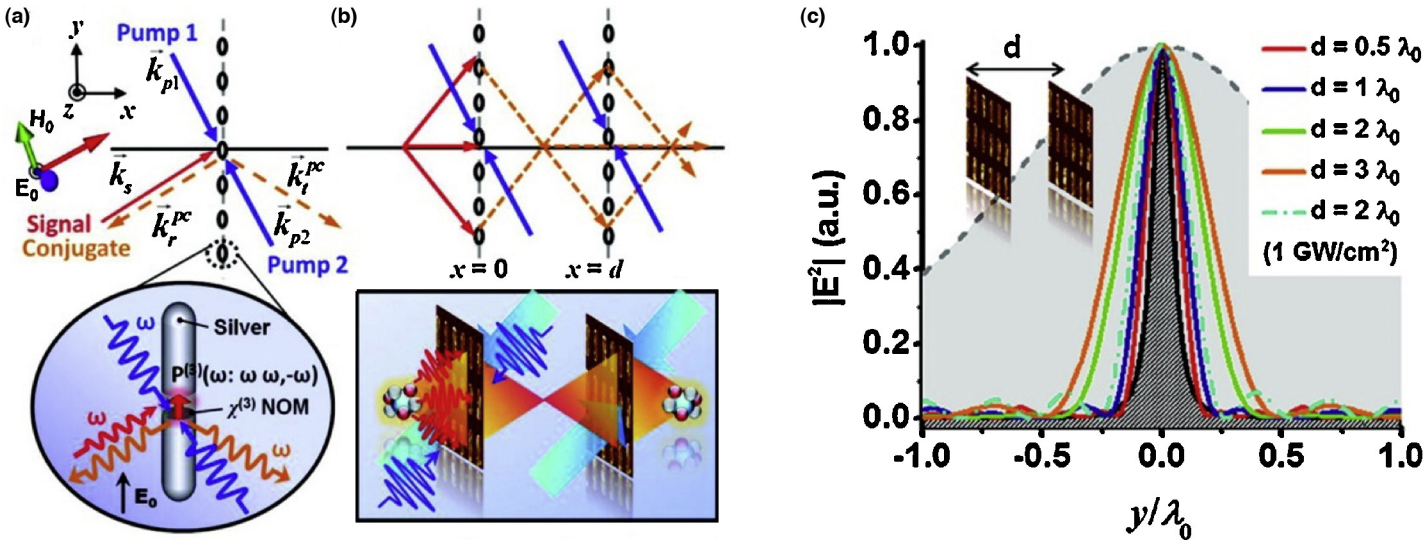

FIGURE 9

A pair of meta-surfaces formed by center-fed half-wavelength antennas for 'perfect' imaging. (a) Schematic of a single center-fed antenna array with signal and pump illuminations. The inset shows the geometry of the single antenna. (b) Schematic of phase conjugating meta-surfaces together with pump illumination directions. (c) Comparison of the imaged field of the source for various separation distances between the two surfaces. The solid black curve displays the sub-wavelength source field distribution, whereas the black dashed curve shows its diffracted field at image plane without meta-surfaces. Figures adapted from Ref. [79].

due to the bistable dependence of feed permittivity upon intensity.

The center-fed half-wavelength antenna has been further suggested for a realization of phase-conjugating surfaces [79]. A pair of ideal phase conjugating meta-surfaces was proposed to mimic a negative index slab in order to achieve perfect lensing [59,80]. A meta-surface was created by a periodic array of center-fed dipole antennas as shown in Fig. 9a,b. The surface was illuminated by a monochromatic signal wave and two counter propagating pumps at the same frequency such that their propagation vectors are equal and opposite in direction. In such a scheme, the phase-matching condition in FWM process caused by a cubic nonlinearity requires a dipole to be generated in the nonlinear load having a conjugated phase with respect to the incident signal. The transmitted signal is then cast upon a similar, suitably positioned, meta-surface which once again conjugates the sign of the incident wave to form an image behind the second surface. Figure 9c shows the imaging of a sub-wavelength source for various values of the separation distances between the two antenna surfaces. Also shown for comparison is the original source width (black) and diffracted wave's width (dashed-gray) in the absence of imaging surfaces.

Conclusion

In this contribution we reviewed both well-established trends and recent developments toward the realization and the exploitation of nonlinear effects in plasmonic antennas. This included degenerate intensity-dependent as well as frequency conversion effects that arise in antennas made up of centrosymmetric media due to structural asymmetry. As amply observed, the major advantage of plasmonic antennas lies in their ability to provide high near field intensities due to sub-wavelength focusing of light at resonance. This enhancement yields efficient frequency conversion and nonlinear intensity modulation.

Despite all the promises and possibilities for materializing functional devices at nanoscale, it should be pointed out in fairness that the advantage of plasmonic antennas does not come without a cost. Owing to high metallic absorption, the question always remains as to what extent the nonlinear processes can benefit before the power is dissipated. This problem was addressed at length in an illuminating study by Khurgin *et al.* [81] which suggested that plasmonic antennas are more suitable for applications to be operated at low power thresholds such as frequency conversion and Raman scattering. In contrast, more sophisticated applications where a high input power is required, like switching elements, phase-shifters, etc., might fail to achieve the required efficiency levels for realistic possible pump powers. In general, it can be concluded that whenever a nonlinear response is required to be observed from a smallest possible volume, plasmonic antennas seem to be the devices of choice to strengthen and enhance these effects.

Acknowledgements

Support from the German Federal Ministry of Education and Research (PhoNa), the Thuringian State Government (MeMa), and the German Science Foundation (SPP 1391 Ultrafast Nano-optics) is acknowledged.

References

[1] S.A. Maier, Plasmonics: Fundamentals and Applications, Springer, 2007.
[2] M. Born, E. Wolf., Principles of Optics: Electromagnetic Theory of Propagation, Interference and Diffraction of Light, 7th ed., Cambridge University Press, 1999.
[3] D.K. Gramotnev, S.I. Bozhevolnyi, Nat. Photon. (2010), http://dx.doi.org/10.1038/nphoton.2009.282.
[4] R. Alaee, et al. Nano Lett. (2013), http://dx.doi.org/10.1021/nl4007694.
[5] R.W. Boyd, Nonlinear Optics, 3rd ed., Academic Press, 2008.
[6] S. Kim, et al. Nature (2008), http://dx.doi.org/10.1038/nature07012.
[7] H. Aouani, et al. Nano Lett. (2012), http://dx.doi.org/10.1021/nl302665m.
[8] M. Hentschel, et al. Nano Lett. (2012), http://dx.doi.org/10.1021/nl301686x.
[9] T. Hanke, et al. Phys. Rev. Lett. (2009), http://dx.doi.org/10.1103/PhysRevLett.103.257404.

[10] J.E. Sipe, et al. Phys. Rev. B (1980), http://dx.doi.org/10.1103/PhysRevB.21.4389.
[11] P. Guyot-Sionnest, W. Chen, Y.R. Shen, Phys. Rev. B (1986), http://dx.doi.org/10.1103/PhysRevB.33.8254.
[12] J.I. Dadap, et al. Phys. Rev. Lett. (1999), http://dx.doi.org/10.1103/PhysRevLett.83.4045.
[13] T. Paul, C. Rockstuhl, F. Lederer, J. Mod. Opt. (2011), http://dx.doi.org/10.1080/09500340.2010.511291.
[14] C. Ciracì, et al. Phys. Rev. B (2012), http://dx.doi.org/10.1103/PhysRevB.85.201403.
[15] P. Ginzburg, et al. Phys. Rev. B (2012), http://dx.doi.org/10.1103/PhysRevB.86.085422.
[16] C. Ciracì, et al. Phys. Rev. B (2012), http://dx.doi.org/10.1103/PhysRevB.86.115451.
[17] D. Marinica, et al. Nano Lett. (2012), http://dx.doi.org/10.1021/nl300269c.
[18] R. Esteban, et al. Nat. Commun. (2012), http://dx.doi.org/10.1038/ncomms1806.
[19] J.A. Scholl, et al. Nano Lett. (2013), http://dx.doi.org/10.1021/nl304078v.
[20] D. Pacifici, H.J. Lezec, H.A. Atwater, Nat. Photon. (2007), http://dx.doi.org/10.1038/nphoton.2007.95.
[21] R. Filter, et al. Phys. Rev. B (2012), http://dx.doi.org/10.1103/PhysRevB.86.035404.
[22] D.R.H. Craig, F. Bohren, Absorption and Scattering of Light by Small Particles, Wiley-VCH, 1998.
[23] E. Prodan, et al. Science (2003), http://dx.doi.org/10.1126/science.1089171.
[24] A.I. Fernández-Domínguez, S.A. Maier, J.B. Pendry, Phys. Rev. B (2012), http://dx.doi.org/10.1103/PhysRevB.85.165148.
[25] D.P. Fromm, et al. Nano Lett. (2004), http://dx.doi.org/10.1021/nl049951r.
[26] E. Moreno, et al. J. Opt. Soc. Am. A (2002), http://dx.doi.org/10.1364/JOSAA.19.000101.
[27] C. Rockstuhl, M.G. Salt, H.P. Herzig, J. Opt. Soc. Am. A (2003), http://dx.doi.org/10.1364/JOSAA.20.001969.
[28] K. Busch, M. König, J. Niegemann, Laser Photon. Rev. (2011), http://dx.doi.org/10.1002/lpor.201000045.
[29] H. Urbach, et al. J. Mod. Opt. (2011), http://dx.doi.org/10.1080/09500340.2010.538736.
[30] P. Ginzburg, Nano Lett. (2011), http://dx.doi.org/10.1021/nl200612f.
[31] L. Novotny, Phys. Rev. Lett. (2007), http://dx.doi.org/10.1103/PhysRevLett.98.266802.
[32] J. Dorfmüller, et al. Nano Lett. (2010), http://dx.doi.org/10.1021/nl101921y.
[33] A. Alú, N. Engheta, Nat. Photon. (2008), http://dx.doi.org/10.1038/nphoton.2008.53.
[34] J. Pendry, et al. IEEE Trans. Microw. Theor. Tech. (1999), http://dx.doi.org/10.1109/22.798002.
[35] C. Rockstuhl, et al. Opt. Express (2006), http://dx.doi.org/10.1364/OE.14.008827.
[36] A.M. Moran, et al. J. Phys. Chem. B (2005), http://dx.doi.org/10.1021/jp046704.
[37] J. Nappa, et al. J. Chem. Phys. (2006), http://dx.doi.org/10.1063/1.2375095.
[38] J. Butet, et al. Phys. Rev. Lett. (2010), http://dx.doi.org/10.1103/PhysRevLett.105.077401.
[39] G. Bachelier, et al. Phys. Rev. B (2010), http://dx.doi.org/10.1103/PhysRevB.82.235403.
[40] Y. Pu, et al. Phys. Rev. Lett. (2010), http://dx.doi.org/10.1103/PhysRevLett.104.207402.
[41] S. Wunderlich, U. Peschel, Opt. Express (2013), http://dx.doi.org/10.1364/OE.21.018611.
[42] J. Butet, et al. J. Phys. Chem. C (2013), http://dx.doi.org/10.1021/jp310169u.
[43] J. Richter, et al. Plasmonics (2013), http://dx.doi.org/10.1007/s11468-012-9429-2.
[44] C. Hubert, et al. Appl. Phys. Lett. (2007), http://dx.doi.org/10.1063/1.2734503.
[45] B. Metzger, et al. Opt. Lett. (2012), http://dx.doi.org/10.1364/OL.37.004741.
[46] J. Berthelot, et al. Opt. Express (2012), http://dx.doi.org/10.1364/OE.20.010498.
[47] S. Kujala, et al. Phys. Rev. Lett. (2007), http://dx.doi.org/10.1103/PhysRevLett.98.167403.
[48] H. Husu, et al. Nano Lett. (2012), http://dx.doi.org/10.1021/nl203524k.
[49] M.W. Klein, et al. Science (2006), http://dx.doi.org/10.1126/science.1129198.
[50] N. Feth, et al. Opt. Lett. (2008), http://dx.doi.org/10.1364/OL.33.001975.
[51] S. Linden, et al. Phys. Rev. Lett. (2012), http://dx.doi.org/10.1103/PhysRevLett.109.015502.
[52] A. Slablab, et al. Opt. Express (2012), http://dx.doi.org/10.1364/OE.20.000220.
[53] B.-L. Wang, et al. J. Appl. Phys. (2012), http://dx.doi.org/10.1063/1.4759051.
[54] G.F. Walsh, L. Dal Negro, Nano Lett. (2013), http://dx.doi.org/10.1021/nl401037n.
[55] Y. Zhang, et al. Proc. Natl. Acad. Sci. U. S. A. (2013), http://dx.doi.org/10.1073/pnas.1220304110.
[56] K. Thyagarajan, J. Butet, O.J.F. Martin, Nano Lett. (2013), http://dx.doi.org/10.1021/nl400636z.
[57] J.I. Dadap, J. Shan, T.F. Heinz, J. Opt. Soc. Am. B (2004), http://dx.doi.org/10.1364/JOSAB.21.001328.
[58] H. Husu, et al. Opt. Express (2010), http://dx.doi.org/10.1364/OE.18.016601.
[59] J.B. Pendry, Phys. Rev. Lett. (2000), http://dx.doi.org/10.1103/PhysRevLett.85.3966.
[60] S. Kujala, et al. Opt. Express (2008), http://dx.doi.org/10.1364/OE.16.017196.
[61] J. Petschulat, et al. Phys. Rev. A (2009), http://dx.doi.org/10.1103/PhysRevA.80.063828.
[62] M.W. Klein, et al. Opt. Express (2007), http://dx.doi.org/10.1364/OE.15.005238.
[63] B. Luk'yanchuk, et al. Nat. Mater. (2010), http://dx.doi.org/10.1038/nmat2810.
[64] S.G. Rodrigo, H. Harutyunyan, L. Novotny, Phys. Rev. Lett. (2013), http://dx.doi.org/10.1103/PhysRevLett.110.177405.
[65] H. Harutyunyan, et al. Phys. Rev. Lett. (2012), http://dx.doi.org/10.1103/PhysRevLett.108.217403.
[66] K. Thyagarajan, et al. Opt. Express (2012), http://dx.doi.org/10.1364/OE.20.012860.
[67] S.B. Hasan, et al. Phys. Rev. B (2013), http://dx.doi.org/10.1103/PhysRevB.88.205125.
[68] M. Navarro-Cia, S.A. Maier, ACS Nano (2012), http://dx.doi.org/10.1021/nn300565x.
[69] S.B. Hasan, et al. Phys. Rev. B (2011), http://dx.doi.org/10.1103/PhysRevB.84.195405.
[70] H. Gibbs, et al. in: H. Walther, K. Rothe (Eds.), Laser Spectroscopy IV, Volume 21 of Springer Series in Optical Sciences, Springer, Berlin, Heidelberg, 1979, pp. 441–450.
[71] P.-Y. Chen, A. Alù, Phys. Rev. B (2010), http://dx.doi.org/10.1103/PhysRevB.82.235405.
[72] P.-Y. Chen, M. Farhat, A. Alù, Phys. Rev. Lett. (2011), http://dx.doi.org/10.1103/PhysRevLett.106.105503.
[73] M. Abb, et al. Nano Lett. (2011), http://dx.doi.org/10.1021/nl200901w.
[74] G.A. Wurtz, et al. Nat. Nano (2011), http://dx.doi.org/10.1038/nnano.2010.278.
[75] C. Argyropoulos, et al. Phys. Rev. Lett. (2012), http://dx.doi.org/10.1103/PhysRevLett.108.263905.
[76] T. Kosako, Y. Kadoya, H.F. Hofmann, Nat. Photon. (2010), http://dx.doi.org/10.1038/nphoton.2010.34.
[77] T. Coenen, et al. Nano Lett. (2011), http://dx.doi.org/10.1021/nl201839g.
[78] I.S. Maksymov, A.E. Miroshnichenko, Y.S. Kivshar, Opt. Express (2012), http://dx.doi.org/10.1364/OE.20.008929.
[79] P.-Y. Chen, A. Alù, Nano Lett. (2011), http://dx.doi.org/10.1021/nl203354b.
[80] S. Maslovski, S. Tretyakov, J. Appl. Phys. (2003), http://dx.doi.org/10.1063/1.1604935.
[81] J.B. Khurgin, G. Sun, Opt. Express (2013), http://dx.doi.org/10.1364/OE.21.027460.